IOP Publishing Journal of Micromechanics and Microengineering
J. Micromech. Microeng. **25** (2015) 105008 (11pp) doi:10.1088/0960-1317/25/10/105008

Miniature proportional control valve with top-mounted piezo bimorph actuator with millisecond response time

Maarten S Groen[1], Dannis M Brouwer[2], Joost C Lötters[1,3] and Remco J Wiegerink[1]

[1] MESA$^+$ Institute for Nanotechnology, University of Twente, Drienerlolaan 5, 7522 NB Enschede, The Netherlands
[2] Mechanical Automation and Mechatronics, University of Twente, Drienerlolaan 5, 7522 NB Enschede, The Netherlands
[3] Bronkhorst High-Tech B.V., Nijverheidsstraat 1A, 7261 AK Ruurlo, The Netherlands

E-mail: M.S.Groen@utwente.nl

Received 23 April 2015, revised 17 July 2015
Accepted for publication 27 July 2015
Published 9 September 2015

Abstract

In this paper we demonstrate the realization of a micro control valve with a top-mounted piezoelectric bimorph actuator, to obtain a high-bandwidth proportional control valve for gases in the range of several grams per hour. Dynamic fluidic and mechanical characterization shows that the valve is suitable for high-speed flow control with response times on the order of milliseconds. The microvalve contains an integrated capacitive displacement sensor for position-based control, which can be used to improve the control precision. The microvalve is realized in a straight-forward fabrication process based on a single SOI wafer. A high level of integration of the piezo actuator is achieved using a flexible silicone rubber support between the bimorph and the silicon. This leads to a small volume, high speed device.

Keywords: microvalve, piezoelectric actuation, capacitive sensing, MEMS, piezoelectric bimorph, actuator integration

(Some figures may appear in colour only in the online journal)

1. Introduction

In many fields relating to microfluidics there is a demand for accurate, proportional control of fluid flow. This control could for example relate to total fluid sample size in analytical systems [1, 2], constant flow of reactants in reaction chemistry [3, 4], or automated drug administration in medicine [5]. The key requirement here is the ability to control flow to a specified value, rather than on-off control (bistable valves) or passive one-way control (flow rectifiers). One of the primary requirements for a proportional micro control valve is therefore the integration of a small-scale actuator that can regulate the valve state repeatably. Important demands for proportional flow control systems include short response times (on the order of milliseconds), high control precision (low hysteresis), low power usage (on the order of tens of milliwatts) and small device dimensions ($<1\,\mathrm{cm}^3$). Another important requirement is high design simplicity, since reliable and low-cost fabrication becomes more difficult to realize at small scales.

A large number of microvalves have been presented in literature, but only a fraction of them are suitable for proportional control and even fewer allow full integration of a miniaturized actuator [6–8]. Unfortunately most of those devices are still relatively large, with particularly the actuator requiring larger volumes. The two most common actuator types that allow high-speed proportional control are electromagnetic and piezoelectric actuation. Electromagnetic actuation suffers from decreasing work densities at smaller scales, which is why piezoelectric actuation is commonly applied in downscaling scenarios [8]. Nevertheless device dimensions are often on the order of centimeters, mostly because stacked piezos are used which have a very small stroke per unit length [9–17].

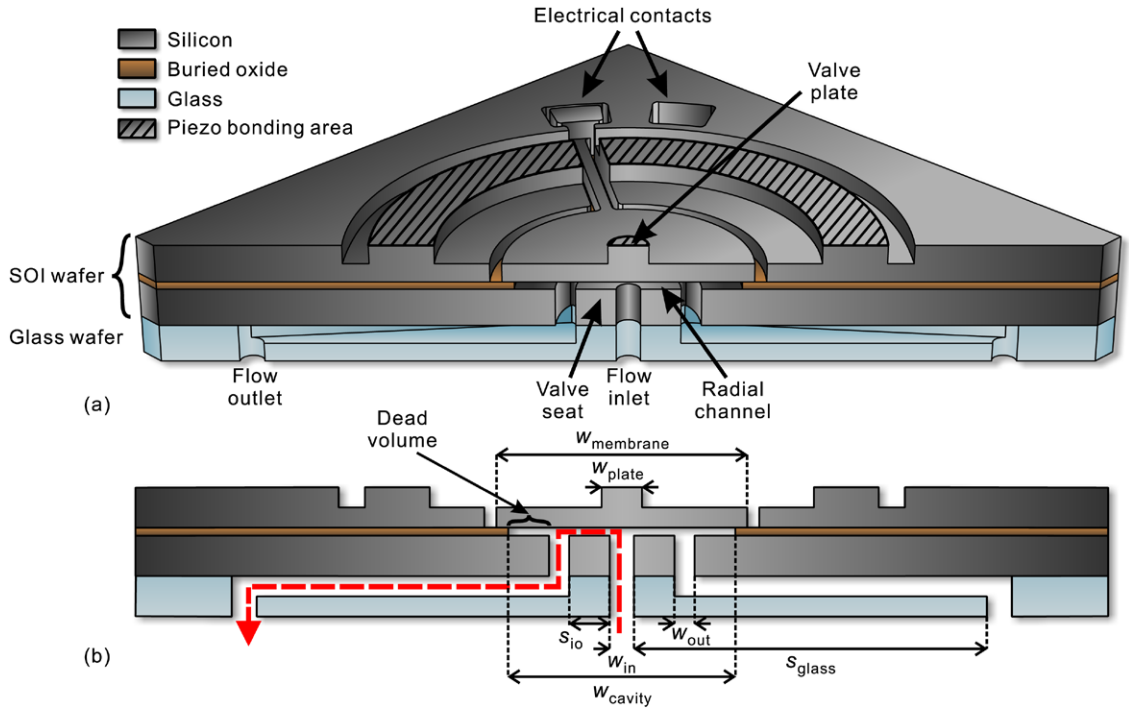

Figure 1. Artist impression and operating principle of the SOI-based microvalve. Flow is regulated by vertical translation of the valve plate with regards to the valve seat. The electrical contact points allow capacitive displacement sensing of the valve membrane. Gas flow is indicated by the red arrow.

Gap-closing electrostatic actuation is also commonly applied, as it offers high speeds at small volumes, but its highly nonlinear control characteristics usually limit it to bistable operation [18].

Although small-volume microvalves with response times on the order of milliseconds have been reported in literature [10, 19, 20], they often suffer from complex fabrication processes, poor control precision or hysteresis. A relatively simple design using a stack piezo actuator was fabricated in a two-wafer fabrication process, but still required seven lithographic mask steps and wafer bonding [11]. We have previously presented a microvalve for proportional control of gas flow, realized in a straight-forward, single wafer fabrication process [21]. In this valve we have demonstrated the use of capacitive displacement sensing to compensate for hysteresis in a piezoelectric actuator. Although the microvalve itself was realized in a single wafer process, the piezoelectric actuator was mounted on the microvalve using a 3D-printed support structure that required high-precision manual assembly. This made it unsuitable for large scale production and increased the device dimensions to centimeter scale. Additionally, the reported valve design lacked a fluidic outlet port, only controlling flow from a fluidic inlet, through the microfluidic chip to atmosphere.

In this paper we present an improved design of this valve, controlling flow between an inlet and outlet. We achieve a high level of integration by replacing the 3D-printed support structure with a miniature bimorph piezoelectric actuator that can be mounted directly onto the fluidic chip. In our experiments it is found that direct adhesive bonding of the piezo bimorph to the silicon causes a severe reduction in the piezo displacement. This problem is analyzed using finite element modeling and a solution is found and implemented using a support ring of flexible material between the piezo and the silicon. The realized micro control valve is validated with fluidic and mechanical characterization measurements.

2. Analysis

2.1. Design and operating principle

Figure 1 shows the basic design of the microvalve, based on the design described in [21]. It consists of a circular valve plate suspended above the valve seat by a closed, flexible membrane, such that a radial flow channel exists between the valve plate and the valve seat. The height of the radial channel changes by vertical movement of the plate, changing the flow resistance of the valve. An electrical capacitance C_{valve} exists between the plate and the seat, bearing an inverse relationship with their separation S:

$$C_{\text{valve}} \approx \frac{\epsilon_0 \cdot \epsilon_r \cdot A}{S} + C_{\text{par}}. \tag{1}$$

Where ϵ_0 is the vacuum permittivity, ϵ_r is the dielectric constant of the medium between the plate and the seat, A is the surface area of the valve membrane and C_{par} is the constant, parasitic capacitance arising from the immovable parts of the valve membrane. Since capacitance can be measured without waiting for flow stabilization, this makes it possible to use the capacitance as a high-speed control signal for position based valve control. At the same time the capacitive sensor can be used to compensate for hysteresis in the actuator.

Table 1. Summary of the valve dimensions.

Parameter	Variable	Value
Wafers:		
Device layer thickness	t_{DL}	50 μm
Handle layer thickness	t_{HL}	400 μm
Buried oxide thickness	t_{BOX}	4 μm
Glass wafer thickness	t_{glass}	525 μm
Valve:		
Membrane width	$w_{membrane}$	4.6 mm
Membrane thickness	$t_{membrane}$	25 μm
Plate width	w_{plate}	800 μm
Plate thickness	t_{plate}	50 μm
Cavity width	w_{cavity}	3.5 mm
Fluidic connections:		
Inlet channel width	w_{in}	600 μm
Outlet channel width	w_{out}	$>$ 500 μm
Inlet-outlet spacing	s_{io}	500 μm
Glass inlet-outlet spacing	s_{glass}	8.7 mm

Like the previously reported valve design, the valve is realized in a silicon-on-insulator (SOI) wafer. Apart from simplifying the fabrication process, this has the advantage that the valve plate and seat both have a low surface roughness, which is beneficial for the leakage performance when the valve is closed. The valve plate is formed in the SOI device layer and the inlet and outlets are shaped in the handle layer. The buried oxide (BOX) between the valve plate and valve seat is removed as a sacrificial layer, leaving the valve plate free to move up and down.

In contrast to the previous design, both the valve inlet and outlets are on the bottom side of the chip. This means that extra care must be taken to prevent leakage paths from inlet to outlet during interfacing of the fluidic chip. However, the distance between inlet and outlet channels can not be made arbitrarily large, as this would increase the etching time of the BOX layer and increase the valve's dead volume (see figure 1(b)). To allow easier assembly of the microvalve chip to a fluidic chipholder, a glass support wafer is added that increases the inlet to outlet spacing. Note that this wafer is not required for correct operation of the valve and may be replaced with other fluidic components, depending on the application.

2.2. Valve dimensions

The dimensions noted in figure 1b are summarized in table 1. The valve membrane diameter is $w_{membrane} = 4.6$ mm, with the valve plate in the center defined as $w_{plate} = 800$ μm. The circular flow inlet is situated beneath the valve plate, with a diameter of $w_{in} = 600$ μm. This width is chosen far greater than the height of the radial channel, to ensure that the flow resistance of the inlet channel is negligible compared to the valve resistance. Similarly the flow outlets are made to be $w_{out} > 500$ μm wide. The inlet to outlet spacing is chosen to be $s_{io} = 600$ μm, which is expected to provide enough bonding surface to enable a leak-tight bond between the microvalve chip and the glass support wafer. The inlet-to-outlet spacing of the glass support wafer is $s_{glass} = 8.7$ mm.

Table 2. Specifications of the T216-A4NO-273X bimorph actuator.

Parameter	Variable	Value
Mechanical:		
Monomorph thickness	t_{mono}	190 μm
Total thickness	t_{piezo}	410 μm
Diameter	w_{piezo}	12.7 mm
Stiffness	K_{piezo}	125 kN m^{-1}
Resonance frequency	f_{piezo}	7.3 kHz
Piezoelectric:		
Rated voltage (AC)	V_{max}	$\pm$180 V
Free stroke	S_{free}	$\pm$19.1 μm
Blocking force	F_{block}	$\pm$2.4 N

The valve membrane thickness is chosen to be $t_{membrane} = 25$ μm thick, which is half the starting thickness of the device layer. This ensures that mechanical contact between the valve membrane and the piezo actuator occurs only at the central plate, so that the valve membrane remains free to deform. FEM analysis shows that at 25 μm thickness the membrane can be displaced tens of micrometers at very low forces ($<$2 mN). Maximum bending stress remains very low, on the order of tens of megapascals. Note that the valve membrane is physically isolated from the surrounding device layer silicon, to reduce the constant parasitic capacitance in the valve.

The size of the valve cavity underneath the membrane depends on the etching time of the BOX layer, and is approximately $w_{cavity} \approx 3.5$ mm for the chosen inlet to outlet pitch. At these dimensions, the dead volume of the valve at its resting position remains small at approximately 12 nL.

The thickness of the BOX layer determines the required actuator stroke to fully close the valve, but also determines the maximum valve separation and therefore the maximum flow supported by the valve. Since our previous valve design applied a monodirectional actuator, the valve plate could not be pulled above the 4 μm BOX layer thickness and flow was limited to approximately 15 sccm at 500 mbar of pressure [21]. With the integration of a bidirectional piezo actuator, our new design will open to at least twice the BOX thickness. Since radial flow scales with the third power of the separation (in the viscous, laminar regime) [22], we estimate that in order to reach a total flow of 200 sccm at 500 mbar a channel height of approximately 10 μm is required. To make sure the actuator can always close the valve entirely, the buried oxide thickness is chosen to be 4 μm thick, and the required actuator stroke becomes $\pm$6 μm.

2.3. Piezo integration

We use T216-A4NO-273X bimorph disks by Piezo Systems Inc. as piezoelectric actuators for our microvalve. The specifications of these actuators are summarized in table 2. The free stroke S_{free} is well above the minimum required displacement of $\pm$6 μm. However, initial experiments revealed that the performance of the actuator diminished severely when it was adhesively bonded to the silicon surface. The maximum stroke was reduced to approximately 1 μm, making it impossible for the valve to close fully.

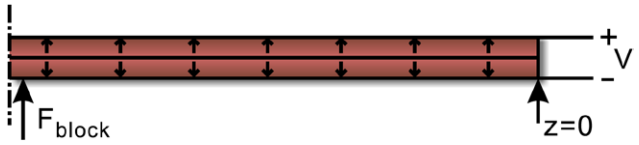

Figure 2. Axisymmetric model used for FEM analysis of the piezo actuator, consisting of two oppositely poled monomorph layers with a prescribed displacement $z = 0$ at the outer edge. Rotational symmetry axis is marked by the dashed line to the left.

This efficiency loss occurs because the adhesive bonding forms a fixed constraint for the piezo across the bonding area, which keeps both monomorph layers from contracting and expanding fully. In order to reach a large stroke, the piezo bimorph requires a support that is flexible in radial direction and allows rotation of the piezo at or near the outer edge. We have therefore designed a flexible piezo support structure, consisting of a ring of flexible material that is placed between the piezo disk and the silicon surface. The flexible support can expand and contract to accommodate expansion and contraction of the piezo bimorph. The ring support can also bend to allow the piezo to rotate, effectively transforming the fixed constraint into a pinned constraint.

We have used finite element (FEM) analysis in COMSOL Multiphysics® v.4.3a to study the critical parameters of this flexible ring support and determine their optimum values to maximize the stroke of the piezo actuator.

3. FEM Analysis

3.1. Piezo model

To create an approximate FEM model of the piezo actuator, we focused on its specified mechanical stiffness, blocking force and free stroke (see table 2), as together they describe both the mechanical and piezoelectric behavior. Figure 2 shows the radially symmetric model used for the analysis. The symmetry axis allows vertical (z-axis) displacement at the center of the piezo, while the piezo's outer bottom edge is constrained with an enforced displacement of $z = 0$. The x, y and rotational axes at the outer edge are unconstrained, leaving the entire piezo free to bend.

We selected COMSOL's built-in PZT-5A material for both piezo layers, and inverted the z-axis of the bottom layer to account for the opposite piezoelectric poling. To match the material properties in our model to the actual piezo actuator (also a PZT-5A ceramic), we varied the bimorph layer thickness until the mechanical stiffness equaled K_{piezo}. This is the case at a monomorph thickness of 168 μm, which is close to the 190 μm thickness of the actual piezo monomorphs.

To obtain the same piezo performance in our model as in the actuator, we varied the electric field applied in the model until the free stroke and blocking force matched the specifications. The free stroke is simply the simulated piezo displacement when no external force is applied. The blocking force equals the boundary load (applied near the center of the disk, left in the image) necessary to push the bimorph back to a fixed surface at its starting position. At an applied electric voltage of 250 V the modeled bimorph reached a free stroke of 20.0 μm at a blocking force of 2.5 N. Since these values match reasonably well with the specifications, the model can be used as a qualitative approximation of the real actuator.

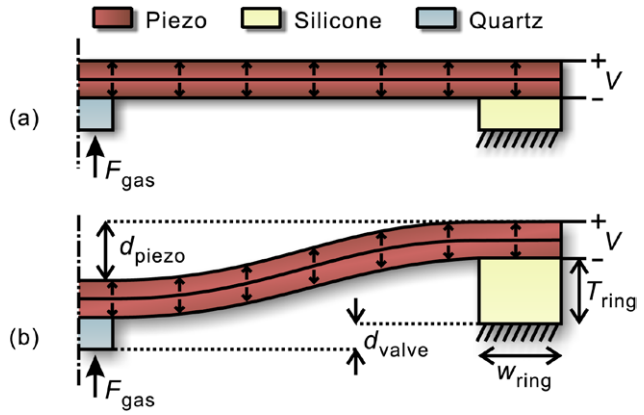

Figure 3. Axisymmetric FEM model of the piezo actuator with a flexible ring support (a). There is a tradeoff between increased piezo displacement and increased stretching of the flexible support due to the gas pressure (b).

3.2. Flexible support model

We have studied the effects of a flexible ring support mounted between the piezo actuator and the silicon microvalve, using the axisymmetric COMSOL model shown in figure 3(a). The piezo model described in the previous section is used, with a ring of flexible material fixed at the outer edge of the piezo (right side of the image). A cylindrical piece of glass is added in the center, as this will be used to transfer the piezo motion to the microvalve. The bottom of the flexible support is given a fixed constraint, and a boundary load F_{gas} is applied at the glass cylinder:

$$F_{\text{gas}} = P_{\text{gas}} * A_{\text{valve}}. \quad (2)$$

Where A_{valve} is the surface area of the valve membrane.

The flexible support is expected to increase the maximum displacement of the piezo, as it allows the piezo layers to expand and contract without much constraint. At the same time however, the gas pressure P_{gas} pushing up against the valve would cause the flexible support to be stretched upward, raising the piezo and the valve plate with it (see figure 3(b)). This means the net displacement of the valve d_{valve} is smaller than the displacement of the piezo d_{piezo}. It is expected that an optimum exists for the flexibility of the support layer, where the net valve displacement is maximized.

Note that in reality an adhesive layer exists between the piezo and the support, which can be modeled using the thin elastic layer boundary condition in COMSOL. It is however found that inclusion of this thin elastic layer has no significant effect on the simulation results, which is in line with the adhesive layer's flexibility being negligible compared to the flexibility of the support material.

The materials used in our analysis are silicone rubbers, as they are readily available both premade and synthesizable with a range of mechanical properties. The first material is a

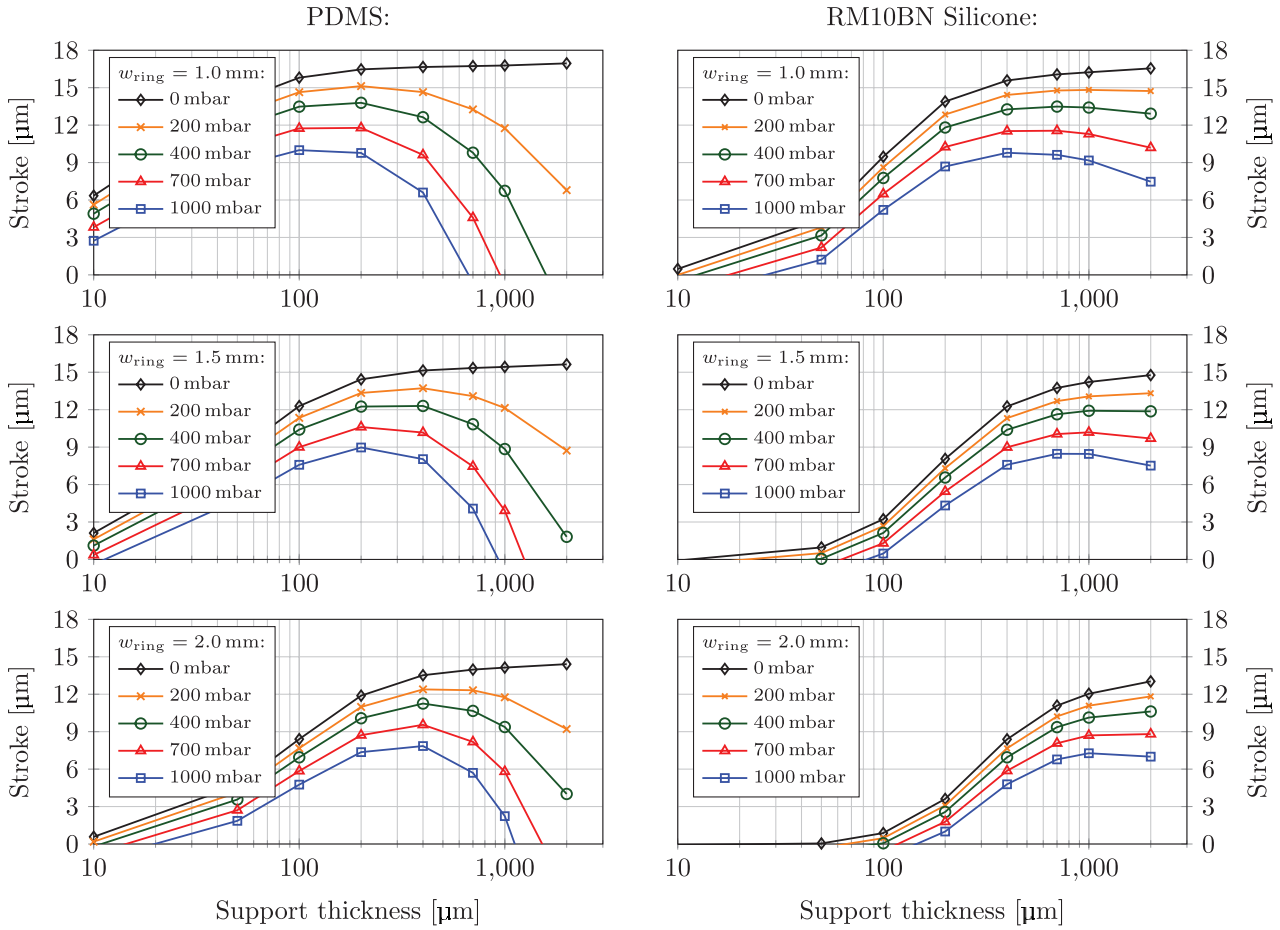

Figure 4. Results of FEM analysis of the maximum downward stroke achievable with a piezo actuator with a flexible ring support made of PDMS (left) or RM10BN silicone rubber (right), as a function of ring width and ring thickness. Note that at higher pressures the flexible support is stretched further upwards, decreasing the net stroke of the actuator.

silicone rubber named RM10BN available as premade sheets with a hardness of 60° Shore A, which corresponds to a Young's modulus of approximately 5–10 MPa [23]. The second material is polydimethylsiloxane (PDMS), which is a common elastomer used in microtechnology and can be shaped with lithographic techniques. It has a Young's modulus on the order of hundreds of kilopascals [24].

3.3. Simulation results

We simulated the maximum downward displacement of the piezo as a function of the width of the flexible support ring w_{ring}, the thickness of the material T_{ring}, and the gas pressure P_{gas}. Figure 4 shows the results for PDMS ($E = 750$ kPa) and RM10BN ($E = 10$ MPa) respectively. A Poisson ratio of $\nu = 0.49$ was used for both materials.

It is found that at zero pressure both materials enable a stroke of approximately 17 μm at a support width of 1 mm. As was expected the net stroke decreases as the gas pressure increases, due to the upward stretching of the support material. This stretching effect is stronger in the more flexible PDMS material, which makes the PDMS system most sensitive to gas pressure. Both materials facilitate a maximum stroke of 10 μm at 1 bar of pressure. For the PDMS material this maximum is reached at a width of $w_{ring} = 1$ mm and a thickness of $T_{ring} = 100$ μm. For the RM10BN silicone rubber the maximum lies at $w_{ring} = 1$ mm and $T_{ring} = 400$ μm.

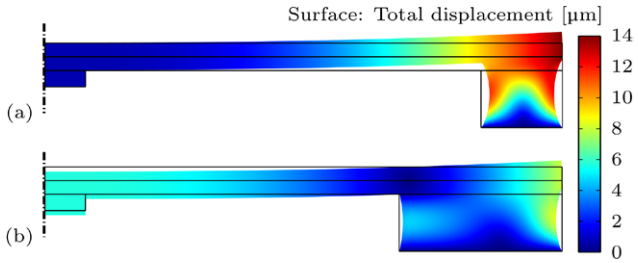

Figure 5. Piezo and ring support deformation results from the FEM model shown in figure 3 at a pressure of 1 bar, showing that the wider ring support (b) is less sensitive to gas pressure. Rotational symmetry axis is marked by the dashed lines to the left.

It is visible in figure 4 that the difference between high pressure stroke and low pressure stroke is larger for slimmer supports. This means that slimmer supports are more susceptible to the gas pressure pushing them up. This can be explained when looking at the material displacement, as shown in figure 5. This result plots the deformation of the piezo and ring support using a voltage of 250 V, a pressure of 1 bar and a ring thickness of 700 μm, using $w_{ring} = 1$ mm and $w_{ring} = 2$ mm. For the slim support (a), the material deformation at the inner and outer support edges are approximately equal. For

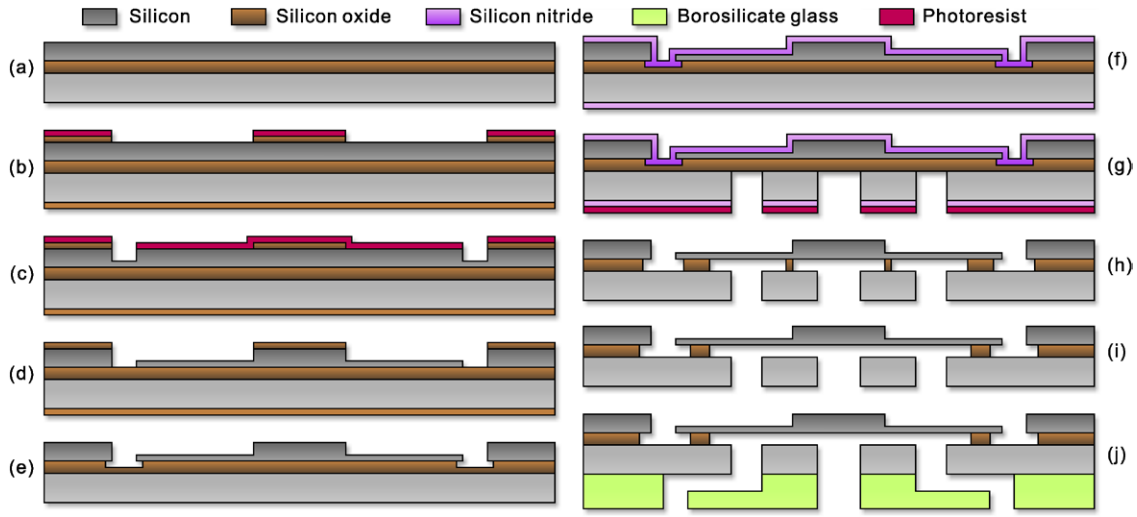

Figure 6. Process flow of the microvalve: (a) SOI wafer; (b) Oxidation and patterning; (c) DRIE of silicon; (d) Resist strip and continued DRIE of silicon; (e) Oxide strip in 50% HF; (f) LPCVD of nitride capping layer; (g) Bottom side DRIE; (h) Etching of BOX and nitride using 50% HF; (i) Etching of BOX using vapor HF; (j) Adhesive bonding to powderblasted glass chips.

the wider ring support (b), the deformation at the inner edge decreases significantly. This is because the inner edge is now close to the 'neutral' pivot point of the piezo, where displacement is zero. Around this point the work done by the piezo is (near) zero, so a wider support does not decrease the piezo's efficacy. It does however increase the total stiffness in the normal direction, meaning this wider support will be stretched less easily by the gas pressure.

Apart from decreasing the sensitivity to gas pressure, a wider ring support simplifies handling and bonding during assembly of the valve. In this work we have therefore chosen to apply premade RM10BN silicone rubber sheets with the ring support as wide as possible. The thickness is chosen at 1 mm, primarily to leave room for electrical wiring to the bottom of the piezo (see figure 8). At this thickness, the maximum stroke at 1 bar pressure in our FEM model is relatively insensitive to support ring width. This allows us to choose a support width of 2 mm.

4. Fabrication

4.1. Microfluidic chip

The fabrication process of the microvalve chips is based on the process described in [21] and illustrated in figure 6. We start with a <1 0 0>-oriented SOI wafer with a 50 μm device layer, 4 μm BOX layer and 400 μm handle layer (figure 6(a)). Both device layer and handle layer are highly doped with a resistivity of 0.005–0.020 Ω cm, to enable electrical sensing of the valve capacitance. A 1 μm thick oxide layer is grown on the wafer using wet thermal oxidation, which is then patterned and etched in a buffered HF solution (7 : 1 HF:NH_4F solution, figure 6(b)). This patterned oxide will act as an etching barrier in subsequent dry etching steps.

A second lithographic pattern is created on the device layer using photoresist, and the silicon is etched with an Alcatel AMS100 deep reactive ion etcher (DRIE) using a Bosch process, to a depth of approximately 30 μm (c). The photoresist is then stripped and a second DRIE step is performed until the shallow structures are etched approximately 25 μm. This also etches the deep structures down to the BOX layer (d). The oxide mask is then removed using a 50% HF solution (e). To protect the exposed BOX layer from subsequent HF etch steps, a 1 μm silicon-rich nitride layer is grown using LPCVD (f). The handle layer is then patterned and etched with a Bosch DRIE process to create the flow inlets and outlets (g).

The valve membrane is released using a combination of liquid and vapor phase HF etching. First the majority of the buried oxide underneath the valve membrane is etched using a 50% HF solution, carefully timed to leave a small amount of oxide separating the valve plate and valve seat (h). This oxide prevents stiction by capillary force during wafer drying. Note that the protective silicon nitride layer is also etched in this step. The wafer is then diced and the individual microfluidic chips are cleaned and dried. After drying the remaining oxide is removed using a vapor phase HF step (i).

To create the glass support chip, a 500 μm thick borosilicate glass wafer is patterned on both side with photoresist foil and powderblasted from both sides, leaving approximately 300 μm deep channels. After cleaning the glass wafer is diced into separate chips. Figure 7 shows a SEM close-up of a realized valve, showing the valve plate, the valve membrane and the deeply etched ring separating the membrane and the surrounding device layer silicon.

4.2. Assembly

The glass and silicon chips are bonded together individually, using Loctite 358 high-viscosity, UV curable adhesive. The bonding process is similar to the method presented in [25]. A thin layer of adhesive is distributed on the glass chip surface using a rubber roller, after which the silicon chip is manually aligned and brought into contact with the glass chip. The transparent glass allows easy verification of both the alignment and

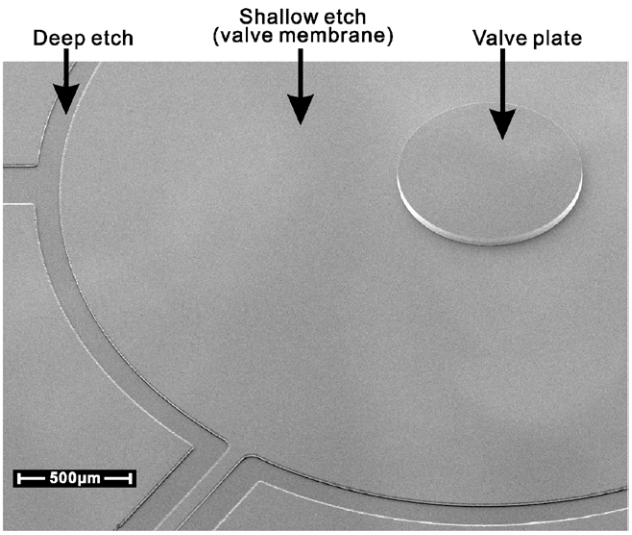

Figure 7. SEM image of the valve membrane, showing both shallow and deep etched structures. The beam visible at the bottom left is for connecting the capacitive readout.

the mechanical contact between the two chips. The chips are then placed in a UV exposure system to cure the adhesive, creating a solid, leak-tight seal between glass and silicon (figure 6(j)).

The flexible ring support is cut out of 1 mm thick RM10BN silicone rubber sheets and gaps are cut into the ring to create room for the piezo wiring (see figure 8). The flexible support is mounted on the silicon using Loctite 4850 flexible cyanoacrylate adhesive. Loctite 480 toughened cyanoacrylate is used to adhesively bond a piece of glass to the valve plate, which will connect the valve plate to the piezo disk. We use diced pieces of a 1 mm glass wafer for this, as they have a well defined thickness.

The piezoelectric actuator is connected on both sides with thin flat cable wires, using silver-based conductive paint for electrical contact and cyanoacrylate adhesive for mechanical fixation. The actuator is then bonded to the silicone ring using Loctite 4850 adhesive, while Loctite 480 is used for the bond between the actuator and the glass connector piece. To connect the microvalve chip to the fluidic characterization system, it is mounted in a fluidic chipholder with Loctite Precision epoxy adhesive. Finally, electrical connections for capacitive sensing are made using platinum wirebonds. A realized microvalve with electrical connections and PMMA chipholder is shown in figure 9.

5. Experiments

5.1. Measurement setup

We have characterized the frequency-dependent electrical and mechanical properties of the microvalve using the measurement scheme illustrated in figure 10. The piezo actuator is driven by a sine voltage at frequencies 1 Hz $\leqslant f_{\mathrm{act}} \leqslant$ 10 kHz), which causes the valve capacitance to change at the same frequency. This capacitive signal is modulated on a sine wave with a frequency of $f_{\mathrm{lock}} = 100$ kHz and 500 $\mathrm{mV_{pp}}$ peak to peak amplitude, connected to the valve plate (device layer). The valve seat (handle layer) is connected to a charge amplifier, the gain of which can be expressed as:

$$V_{\mathrm{out}} = \frac{C_{\mathrm{valve}}}{C_{\mathrm{f}}} \cdot V_{\mathrm{in}}. \tag{3}$$

Where C_{valve} is the valve capacitance and $C_{\mathrm{f}} = 47$ pF is the feedback capacitance of the amplifier. The output of the charge amplifier is sampled and demodulated by a Stanford Research 830 m lock-in amplifier. To further reduce noise the demodulated signal is measured by a second lock-in amplifier, locked at the actuation frequency. The mechanical displacement is measured at the center of the piezo, using a Polytec MSA-400 vibrometer.

The time-dynamic response provides information about the mechanical switching speed of the valve. Although in an ideal case a time-dynamic fluidic characterization could be performed together with the mechanical experiments, such measurements would show the convolution of the fluidic response of the microvalve with that of the measurement setup. Since the internal volume of our microvalve is very small, it would be very difficult to obtain values that are not heavily dependent on the circumstances in which they are measured. The fluidic response of the valve is therefore characterized in the steady state, to eliminate the influence of the measurement setup.

Fluidic characterization of the realized microvalves is done using a gas pressure controller (Bronkhorst P-602CV) backed by a dry nitrogen gas source, connected to a mass flow meter with a maximum range of 178 sccm (Bronkhorst F-111B). The mechanical response during flow measurements is measured using a loadcell, connected above the center of the piezo actuator (Futek LSM250 at 10.00 V supply voltage).

A spark discharge from the valve's electrical wires was observed at a voltage of 120 V, so for safety reasons the actuation voltage was limited to ±100 V.

5.2. Dynamic response

We have characterized the dynamic response of the microvalve in a range of 1 Hz–10 kHz, at actuation voltages of 1.0 $\mathrm{V_{pp}}$, 3.0 $\mathrm{V_{pp}}$ and 10.0 $\mathrm{V_{pp}}$ and at pressures between 0 mbar and 1000 mbar. Figure 11(a) shows the displacement amplitude measured at the center of the piezo, as well as the total phase shift (at $V_{\mathrm{act}} = 3.0$ $\mathrm{V_{pp}}$) between the actuation signal (output of the function generator) and its mechanical response. The dynamic response was found to be independent on pressure for the measured voltage and pressure ranges up to at least 5 kHz (plots show results at zero pressure). Figure 11(b) plots the peak to peak capacitance change of the displacement sensor, calculated from the output of the charge amplifier using equation (3). The figure also plots the phase shift between the lock-in output and the 3.0 $\mathrm{V_{pp}}$ actuation signal. Note that at very low frequencies ($f < 10$ Hz) the measurement time for each data point is on the order of tens of minutes due to the long integration time of the lock-in amplifier, which leads to increased measurement errors caused by drift in the

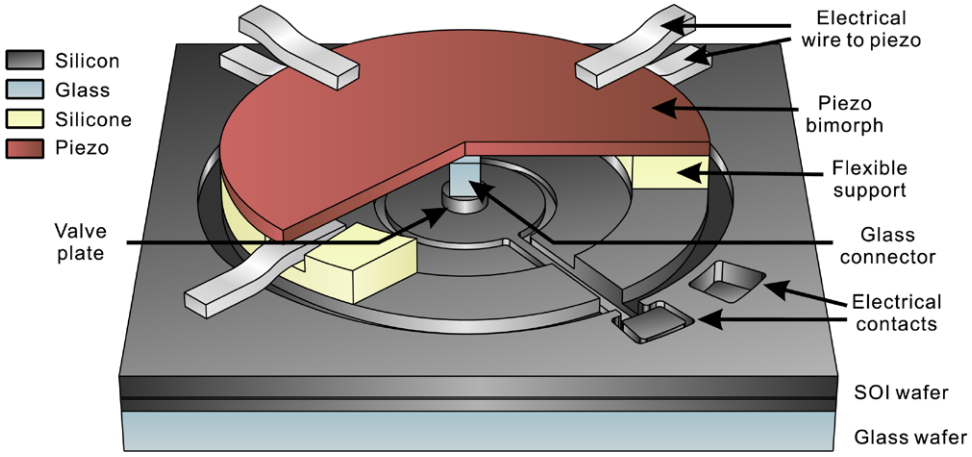

Figure 8. Artist impression of the final assembly of a microfluidic chip with the piezoelectric actuator, using the silicone rubber support.

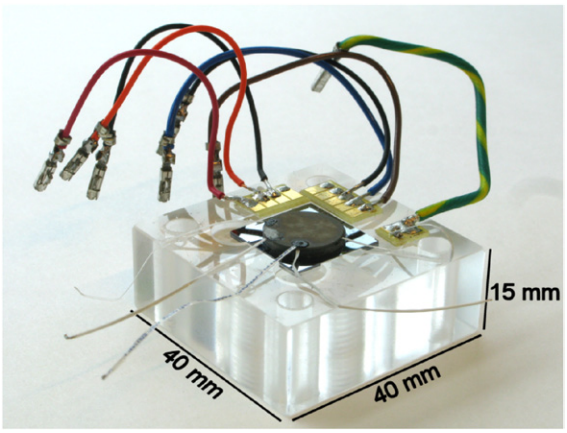

Figure 9. Photograph of the realized microvalve with integrated piezoelectric actuator, mounted on a PMMA fluidic chipholder.

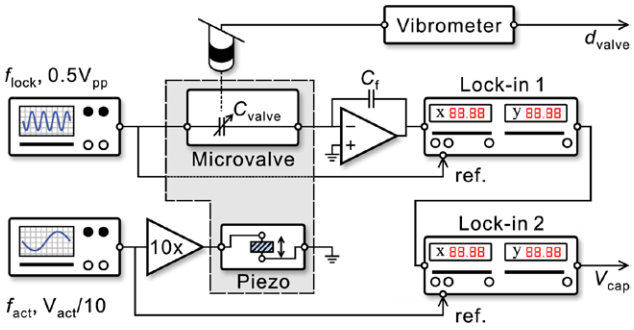

Figure 10. Measurement scheme for the frequency-dependent characterization of the valve's electrical and mechanical properties. The light gray area denotes the microvalve assembly.

piezoelectric actuator. This effect is most notable at the lowest actuation voltages.

In the measured frequency range the microvalve behaves as a second order mass-spring system with a flat amplitude response for frequencies up to 3 kHz, above which the first mechanical resonance (−90° phase shift) is visible at 6.8 kHz. This is close to the specified resonance frequency of the piezo actuator (7.3 kHz). The capacitive displacement sensor (figure 11(b)) shows a flat response up to a bandwidth of approximately 700 Hz. This bandwidth is limited by the sampling rate of the lock-in amplifier, which means that with a dedicated high-speed filter a higher performance should become possible.

At the measured actuation voltages the valve response scales linearly with piezo voltage amplitude. Figure 12 shows the ratio between actuator displacement and actuator voltage (measured in $\mathrm{nm/V_{act}}$) as well as the sensitivity of the capacitive sensor (measured in $\mathrm{V_{cap}}$ $\mu\mathrm{m}^{-1}$). Both plot groups show identical results for all three actuator voltages, which validates the reliability of the capacitive sensor. The above results show that our piezoelectric microvalve is suitable for high-speed flow control with response times on the order of milliseconds. During the course of the measurements the piezo was exposed to (low voltage) AC signals for at least 10^7 cycles. No degradation of piezo performance was observed during this time.

5.3. Steady-state response

Figure 13 shows the steady-state mechanical response of the piezoelectric actuator. The displacement is measured at the center of the piezo as it moves up and down from its neutral position. Note that the constant displacement offset caused by stretching of the ring support is not measured using this method. Apart from this displacement offset the piezo displacement curves are found to be independent of gas pressure, which is in line with the piezo being much stiffer than the support. The maximum piezo displacement drift across all measurements is found to be 4% of full scale. The maximum displacement is ±7.2 μm at ±100 V, which translates to a full stroke of ±13 μm at ±180 V when assuming a continued response as the one shown in figure 13.

The fluidic response of the valve is shown in figure 14, plotting the measured mass flow Q_{mass} as a function of the measured capacitance variation, compensated for the parasitic capacitance ($C_{\mathrm{var}} = C_{\mathrm{valve}} - C_{\mathrm{par}}$). The flow through the fully opened valve exceeds the measurement range of the flow meter at a pressure of 500 mbar. The flow curves in figure 14 show a significant hysteresis, which suggests that the capacitance does not always correspond to a unique value for the valve separation. This is probably caused by a changing tilt angle between the valve plate and valve seat: Mass flow in the

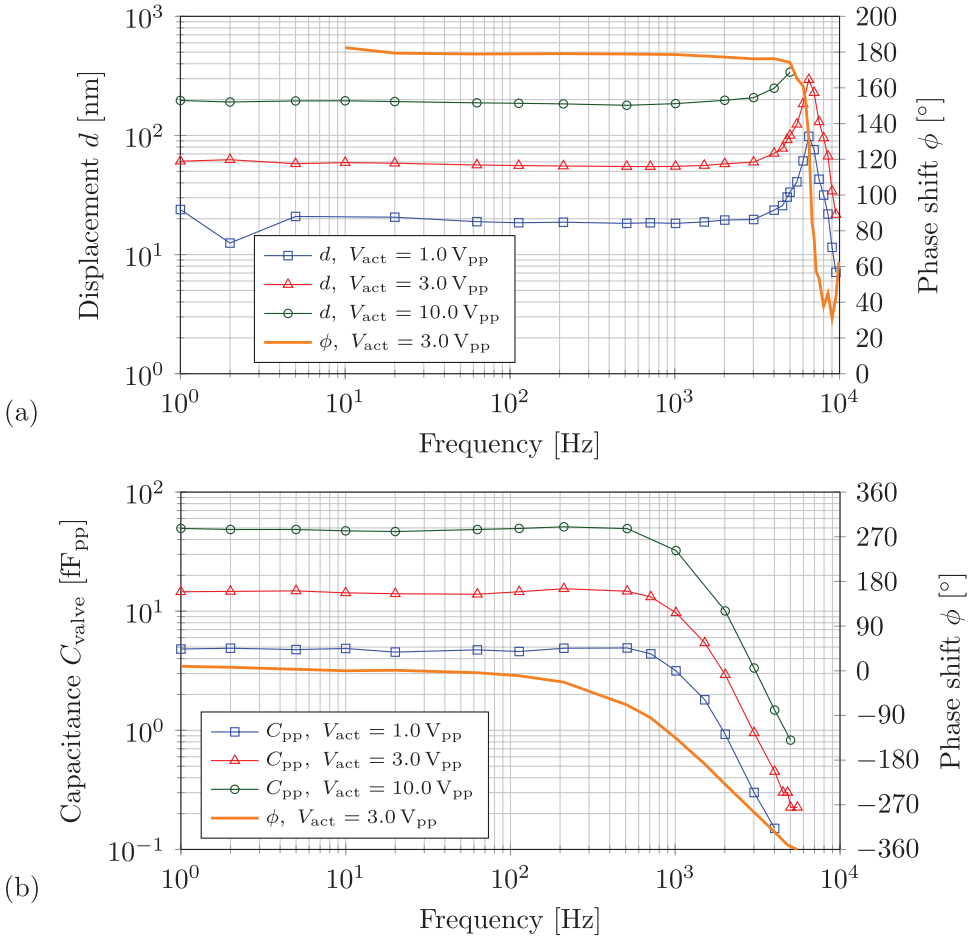

Figure 11. Dynamic response of the microvalve, showing the displacement amplitude at the center of the piezo (a) and the peak-to-peak capacitance variation of the capacitive sensor (b) at various actuation voltages.

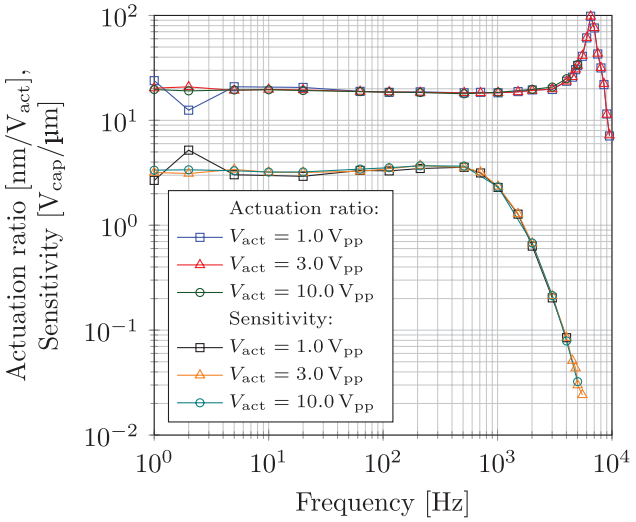

Figure 12. The actuation ratio (displacement per volt) and capacitive sensitivity are nearly independent of actuation voltage across the entire measurement range. Note that the outliers at 1 and 2 Hz are probably caused by piezo drift due to long measurement time.

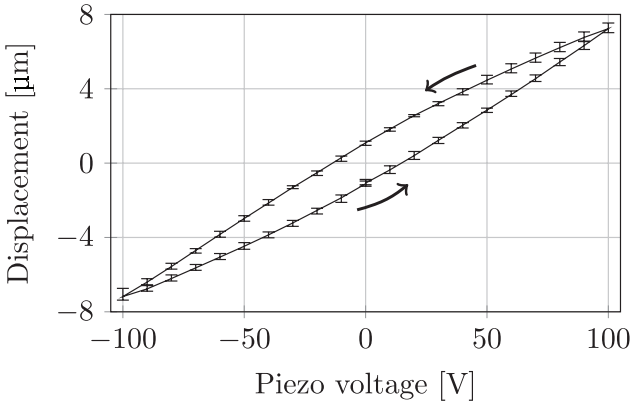

Figure 13. Static mechanical response, average of measurements at pressures of 100, 200, ..., 1000 mbar. Error bars show the minimum and maximum values across all pressures. The total piezo stroke equals ±7.2 μm at ±100 V.

radial channel increases with the third power of the separation [22], and capacitance increases with the inverse of the separation. If the tilt angle changes between opening and closing the valve, this highly non-linear behavior will lead to different mass flows at equal capacitance values, or vice-versa.

Given that the hysteresis loops are closed and repeatable, the valve plate tilt angle must depend on the direction of the piezo movement. This means that the actuator movement is not following the same path in both directions. Because of the top-mounted piezo actuator it is not possible to observe the shape and movement of the valve membrane, for example by

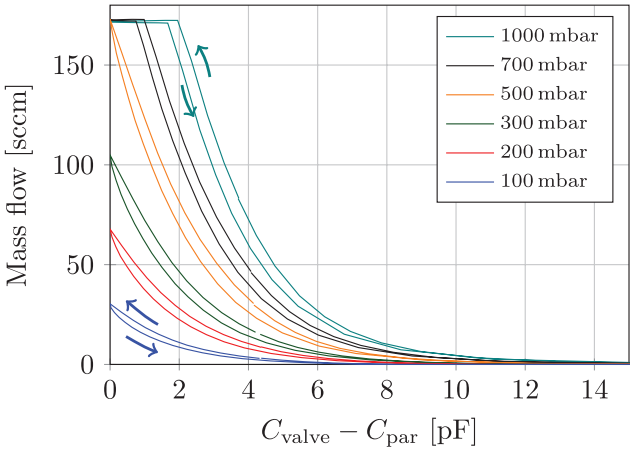

Figure 14. Static fluidic response, showing mass flow as function of valve capacitance, compensated for the parasitic capacitance C_{par}.

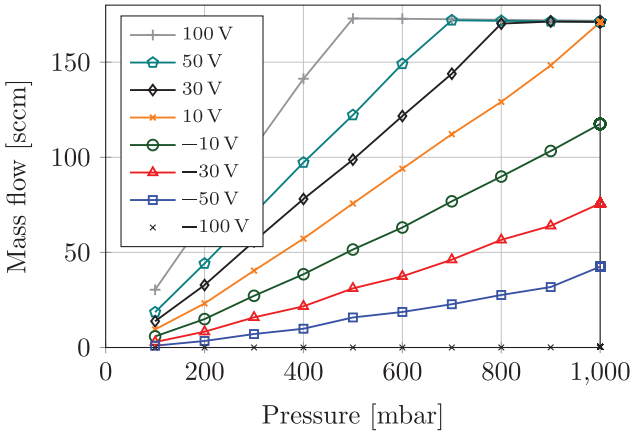

Figure 15. Mass flow as function of pressure, at various actuation voltages. A slight nonlinear increase can be seen at higher pressures, due to stretching of the flexible ring support.

white light interferometry. A possible cause could be a local imperfection in the bond between actuator and support, leading to static and dynamic friction and consequently to mechanical hysteresis. In order to prevent this from happening, care must be taken to provide a reproducible, well-defined connection between valve and actuator, for example by applying surface treatments or by using different materials or adhesives.

Figure 15 shows the measured flow as a function of pressure, at various actuation voltages. The flow scales nearly linearly with pressure with a slight nonlinear increase at higher pressures, probably caused by stretching of the flexible ring support. It is therefore expected that the maximum flow at 1 bar pressure is approximately 350 sccm. If care is taken to prevent electrical discharges at higher voltages, it is possible to increase this flow range further by driving the actuator to its maximum stroke. When the valve is closed the leak flow is below the detection threshold of 0.01 sccm up to a pressure of 500 mbar. At 1 bar the measured leak flow is 0.37 sccm.

6. Conclusions

We have demonstrated the realization of a proportional micro control valve with a top-mounted piezoelectric bimorph actuator. The microvalve is realized in a straight-forward fabrication process based on a single SOI wafer. A glass support wafer was applied to facilitate easier mounting of the microfluidic chip in the experimental setup, but is not required for valve operation. The bimorph actuator is mounted to the microfluidic chip using adhesive bonding. We have achieved a high level of integration of the actuator using a flexible silicone rubber support to maintain maximum actuator stroke. The dimensions of the control valve with actuator are $17 \times 17 \times 1.9$ mm^3. With the addition of the glass support wafer used for fluidic interfacing the thickness increases to 2.4 mm, bringing the total volume of the prototype to 0.69 cm^3.

The valve has been characterized mechanically and fluidically. The system behaves as a second order mass-spring system with a resonance frequency of 6.8 kHz, with a flat mechanical response up to 3 kHz. The capacitive readout was limited by the sampling rate of the lock-in amplifier, with a bandwidth of 700 Hz. These results show that the microvalve is suitable for high-speed flow control with response times on the order of milliseconds.

The valve supports flows up to at least 173 sccm at a pressure of 500 mbar with an expected maximum of 350 sccm at 1 bar, using a maximum actuation voltage of 100 V. This range can be increased by driving the actuator to its full stroke at 180 V. Flow through the valve scales nearly linearly with pressure. The relation between capacitance and flow was found to suffer from hysteresis, which can be attributed to tilting of the valve plate that changes with the direction of the piezo movement. Future work will therefore focus on ensuring a reproducible, well-defined adhesion bond between valve and actuator.

Acknowledgments

The authors would like to thank dr ir R A Brookhuis and ir R G P Sanders (University of Twente) for their valuable contributions. This work was funded by the Point-One Phase2 innovation program of the Dutch Ministry of Economic Affairs (PNE101004).

References

[1] Kovarik M L, Gach P C, Ornoff D M, Wang Y, Balowski J, Farrag L and Allbritton N L 2012 *Anal. Chem.* **84** 516–40
[2] He X, Chen Q, Zhang Y and Lin J-M 2014 *TRAC Trends Anal. Chem.* **53** 84–97
[3] Hessel V, Knobloch C and Lowe H 2008 *Recent Patents Chem. Eng.* **1** 1–16
[4] Wirth T 2013 *Microreactors in Organic Chemistry and Catalysis* (New York: Wiley)
[5] Samad M F and Kouzani A Z 2013 *Microsyst. Technol.* **19** 957–70
[6] Oh K W and Ahn C H 2006 *J. Micromech. Microeng.* **16** R13–39
[7] Henning A K 1998 Microfluidic mems *IEEE Aerospace Conf.* vol 1 pp 471–86
[8] Groen M S, Brouwer D M, Wiegerink R J and Lötters J C 2012 *Micromachines* **3** 396–412

[9] Shoji S, Van der Schoot B, de Rooij N and Esashi M 1991 Smallest dead volume microvalves for integrated chemical analyzing systems *Transducers: Digest of Technical Papers: 1991 Int. Conf. on Solid-State Sensors and Actuators* pp 1052–5
[10] Roberts D C, Li H, Steyn J L, Yaglioglu O, Spearing S M, Schmidt M A and Hagood N W 2003 *J. Microelectromech. Syst.* **12** 81–92
[11] Yang E-H, Lee C, Mueller J and George T 2004 *J. Microelectromech. Syst.* **13** 799–807
[12] Fazal I and Elwenspoek M C 2007 *J. Micromech. Microeng.* **17** 2366–79
[13] Chang C W and Okojie R S 2011 Ni-based microvalves for flow modulation: toward active combustion control *16th Int. Solid-State Sensors, Actuators and Microsystems Conf. Transducers* pp 2434–7
[14] Wu X, Kim S-H, Ji C-H and Allen M G 2011 *J. Micromech. Microeng.* **21** 095003
[15] Mikułowski G, Wiszowaty R and Holnicki-Szulc J 2013 *Smart Mater. Struct.* **22** 125011
[16] Pramanick B, Das S and Bhattacharyya T K 2014 *Sensors Actuators* A **205** 15–25
[17] Zhang D, Lv J, Jiang Y, Chen H and Fu J 2014 *Mechatronics* **24** 511–8
[18] Bae B, Masel R I and Shannon M A 2006 A touch-mode capacitance microvalve equipped with high speed and pressure microsecond switching performance *19th IEEE Int. Conf. on Micro Electro Mechanical Systems* pp 766–9
[19] Rogge T, Rummler Z and Schomburg W K 2004 *Sensors Actuators* A **110** 206–12
[20] Shao P, Rummler Z and Schomburg W K 2004 *J. Micromech. Microeng.* **14** 305–9
[21] Groen M S, Wu K, Brookhuis R A, van Houwelingen M J, Brouwer D M, Lötters J C and Wiegerink R J 2014 A piezoelectric micro control valve with integrated capacitive sensing for ambulant blood pressure waveform monitoring *J. Micromech. Microeng.* **24** 125020
[22] Jackson J D and Symmons G R 1966 *Appl. Sci. Res.* **15** 59–75
[23] Mix A W and Giacomin A J 2011 *Polym.-Plast. Technol. Eng.* **50** 288–96
[24] Armani D, Liu C and Aluru N 1999 Re-configurable fluid circuits by pdms elastomer micromachining *12th IEEE Int. Conf. on Micro Electro Mechanical Systems* pp 222–7
[25] Arayanarakool R, Le Gac S and van den Berg A 2010 *Lab Chip* **10** 2115–21